



HAL
open science

Cool flame chemistry of diesel surrogate compounds: n-decane, 2-methylnonane, 2,7-dimethyloctane, and n-butylcyclohexane

Zhandong Wang, Nils Hansen, Ahren W Jasper, Bingjie Chen, Denisia M Popolan-Vaida, Kiran K Yalamanchi, Ahmed Najjar, Philippe Dagaut, S. Mani Mani Sarathy

► To cite this version:

Zhandong Wang, Nils Hansen, Ahren W Jasper, Bingjie Chen, Denisia M Popolan-Vaida, et al.. Cool flame chemistry of diesel surrogate compounds: n-decane, 2-methylnonane, 2,7-dimethyloctane, and n-butylcyclohexane. *Combustion and Flame*, 2020, 219, pp.384-392. 10.1016/j.combustflame.2020.06.003 . hal-02934457

HAL Id: hal-02934457

<https://hal.science/hal-02934457>

Submitted on 9 Sep 2020

HAL is a multi-disciplinary open access archive for the deposit and dissemination of scientific research documents, whether they are published or not. The documents may come from teaching and research institutions in France or abroad, or from public or private research centers.

L'archive ouverte pluridisciplinaire **HAL**, est destinée au dépôt et à la diffusion de documents scientifiques de niveau recherche, publiés ou non, émanant des établissements d'enseignement et de recherche français ou étrangers, des laboratoires publics ou privés.

Copyright

Cool flame chemistry of diesel surrogate compounds: *n*-decane, 2-methylnonane, 2,7-dimethyloctane, and *n*-butylcyclohexane

Zhandong Wang^{a,b,c*}, Nils Hansen^d, Ahren W. Jasper^e, Bingjie Chen^c, Denisia M. Popolan-Vaida^{f,g,h}, Kiran K. Yalamanchi^c, Ahmed Najjar^c, Philippe Dagautⁱ, S. Mani Sarathy^c

^a State Key Laboratory of Fire Science, University of Science and Technology of China, Hefei, Anhui 230026, PR China

^b National Synchrotron Radiation Laboratory, University of Science and Technology of China, Hefei, Anhui 230029, PR China

^c King Abdullah University of Science and Technology (KAUST), Clean Combustion Research Center (CCRC), Physical Sciences and Engineering Division, Thuwal 23955-6900, Saudi Arabia

^d Combustion Research Facility, Sandia National Laboratories, Livermore, CA 94551, USA

^e Chemical Sciences and Engineering Division, Argonne National Laboratory, 9700 S. Cass Avenue, Argonne, IL 60439, USA

^f Departments of Chemistry, University of California, Berkeley, CA 94720, USA

^g Chemical Sciences Division, Lawrence Berkeley National Laboratory, Berkeley, CA 94720, USA

^h Department of Chemistry, University of Central Florida, Orlando, FL 32816, USA

ⁱ Centre National de la Recherche Scientifique (CNRS), INSIS, ICARE, 1C Avenue de la Recherche Scientifique, 45071, Orléans, cedex 2, France

Abstract: Elucidating the formation of combustion intermediates is crucial to validate reaction pathways, develop reaction mechanisms and examine kinetic modeling predictions. While high-temperature pyrolysis and oxidation intermediates of alkanes have been thoroughly studied, comprehensive analysis of cool flame intermediates from alkane autoxidation is lacking and challenging due to the complexity of intermediate species produced. In this work, jet-stirred reactor autoxidation of four C₁₀ alkanes: *n*-decane, 2-methylnonane, 2,7-dimethyloctane, and *n*-butylcyclohexane, as model compounds of diesel fuel, was investigated from 500 to 630 K using synchrotron vacuum ultraviolet photoionization molecular beam mass spectrometry (SVUV-PIMS). Around 100 intermediates were detected for each fuel. The classes of molecular structures present during the autoxidation of the representative paraffinic functional groups in transport fuels, i.e., *n*-alkanes, branched alkanes, and cycloalkanes were established and were found to be similar from the oxidation of various alkanes. A theoretical approach was applied to estimate the photoionization cross sections of the intermediates with the same carbon skeleton as the reactants, e.g., alkene,

* Corresponding author: E-mail: zhdwang@ustc.edu.cn (Z. Wang)

alkenyl keto, cyclic ether, dione, keto-hydroperoxide, diketo-hydroperoxide, and keto-dihydroperoxide. These species are indicators of the first, second, and third step O₂ addition reactions for the four C₁₀ hydrocarbons, as well as bimolecular reactions involving keto-hydroperoxides. Chemical kinetic models for the oxidation of these four fuels were examined by comparison against mole fraction of the reactants and final products obtained in additional experiments using gas chromatography analysis, as well as the detailed species pool and mole fractions of aforementioned seven types of intermediates measured by SVUV-PIMS. This work reveals that the models in the literature need to be improved, not only the prediction of the fuel reactivity and final products, but also the reaction network to predict the formation of many previous undetected intermediates.

Keywords: autoxidation; peroxides; third sequential O₂ addition; kinetic modeling; synchrotron VUV photoionization molecular beam mass spectrometry

1. Introduction

Concerns on the increasing pollutant and greenhouse gas emissions drive the need for development of clean and efficient engines. Advanced design of engines is dependent on the availability of accurate chemical kinetic models for fuel combustion. Representative mixtures, called surrogates, are often used in engine simulations; they range from single component to multi-component mixtures [1]. The autoxidation characteristics of surrogate fuels at low- to intermediate- temperatures is important for advancing knowledge of analogous processes in advanced low-temperature combustion engines operating in the cool flame regime [2-5]. This study investigates the cool flame chemistry of four C₁₀ hydrocarbons, i.e., *n*-decane, 2-methylnonane (2MNN), 2,7-dimethyloctane (27DMOC), and *n*-butylcyclohexane (NBCH). These hydrocarbons are surrogate compounds for jet fuels and diesel. They represent *n*-alkanes, slightly branched alkanes, and alkylated cycloalkanes [1]. Relative to gasoline surrogate compounds [6], detailed experimental speciation data for diesel surrogate compounds autoxidation is scarce. The major focus of previous

studies has been on global combustion parameters such as ignition delay times, laminar burning velocities and counter flow flames [7-10].

Previous studies measured speciation of *n*-decane oxidation in jet-stirred reactor (JSR) by gas chromatography (GC). The stable intermediates and final products for *n*-decane oxidation from 500-1100 K were measured by Dagaut et al. [11] at 10 atm; the cyclic ethers from the cool flame of *n*-decane were identified. A similar study of *n*-decane oxidation was carried out by Herbinet et al. [12] at atmospheric pressure. More recently, Rodriguez et al. [13] measured more intermediates, e.g. the alkyl hydroperoxide, alkenyl hydroperoxide, and keto-hydroperoxide (KHP) during the autoxidation of *n*-decane. Compared to *n*-decane, JSR oxidation studies for 2-methylnonane, 2,7-dimethyloctane, and *n*-butylcyclohexane are scarce. Previous JSR work has focused on C₆-C₈ hydrocarbons, such as 2-methylhexane [14], 2- and 3-methylheptane [8,15], 2,5-dimethylhexane [16], ethylcyclohexane [17]. The oxidation of *n*-butylcyclohexane was studied in a flow reactor by Natelson et al. [18]. Dozens of stable intermediates like hydrocarbons and oxygenated compounds during the cool flame regime were measured by GC. Herbinet et al. [19] studied the gas-phase oxidation of *n*-butylcyclohexane in a JSR from 500-1100 K, a pressure of 1.067 bar, and equivalence ratio of 0.25-2.0. The pressure effect on the oxidation was also investigated by increasing the JSR pressure up to 10 bar. More than 40 intermediates were measured by GC. These data are valuable to study the reaction mechanism of *n*-butylcyclohexane and develop its kinetic model.

A recent study on *n*-heptane autoxidation showed that cool flame chemistry for this common transportation fuel surrogate is significantly more complex than previously considered in literature [20]. A third sequential of O₂ addition in the low-temperature reaction mechanism, originally observed during the autoxidation of branched alkanes [14,21], was recently confirmed in the autoxidation of various hydrocarbons and oxygenated compounds [22-24]. The propensity of molecules to form highly oxygenated intermediates with 3-5 oxygen atoms was shown to be related to the fuel's molecular structure [22]. The formation of highly oxygenated intermediates with 5 oxygen atoms was also shown to affect ignition delay time simulations since they are additional

radical chain-branching intermediates [25,26]. This discovery was enabled by coupling a JSR with a synchrotron vacuum ultraviolet photoionization molecular beam mass spectrometer (SVUV-PI-MBMS) [27], which are widely used in combustion study [3,28].

The same technique is adopted herein to probe the cool flame intermediates during the autoxidation of *n*-decane, 2-methylnonane, 2,7-dimethyloctane, and *n*-butylcyclohexane. In addition, the autoxidation of these four C₁₀ hydrocarbons was measured by GC and the mole fractions of the reactants and final products were obtained. The systematic study of these four fuels under identical experimental conditions are valuable to (1) study the kinetics of autoxidation of four C₁₀ hydrocarbons, elucidate the cool flame intermediates, and establish the classes of molecular structures of these intermediates; (2) examine literature kinetic models for *n*-decane [7], 2-methylnonane [8], 2,7-dimethyloctane [9], and *n*-butylcyclohexane [29] by comparing against the fuel reactivity, mole fraction of final products and several key autoxidation intermediates, and the detailed species pool; (3) quantify the key intermediates governing auto-ignition and discuss their probable reaction mechanism.

2. Experimental and theoretical methods

The autoxidation of *n*-decane, 2-methylnonane, 2,7-dimethyloctane, and *n*-butylcyclohexane was studied in two fused silica JSR, coupled to different analytic tools for both species measurement and quantification. JSR-1 was coupled to the SVUV-PI-MBMS at the Chemical Dynamics Beamline of Advanced Light Source, Lawrence Berkeley National Laboratory [30]. The flow rate of the fuel was controlled by a syringe pump and mixed with N₂ in a simple vaporizer at a temperature ~ 30 K higher than the boiling point of the fuels. The flow of N₂ and O₂ was controlled by mass flow controllers (MKS). The mass spectrometer has a detection limit of 1 ppm, a mass resolving power of ~ 3500 , and a dynamic range of six orders of magnitude. This allows to distinguish the hydrocarbon and oxygenated species with same nominal mass.

The intermediate species distribution from autoxidation of the four hydrocarbons was measured in 500-630 K range. The experimental conditions were kept the same for the four

hydrocarbons, i.e., fuel initial mole fraction of 0.008, equivalence ratio of 1.0, residence time of 2 s, and pressure of 760 Torr. The design of the JSR-1 with a volume of 33.5 cm³ is similar to that of Dagaut et al. [31], while the sampling of the products was achieved by molecular beam via a quartz nozzle at the outlet of the reactor [27]. The temperature of the reactor was controlled by an oven and monitored by a K-type thermocouple at the outlet of the reactor. The uncertainty on the reactor temperature was ± 20 K, due to the heat loss to the environment and cooling effect of the sampling nozzle [21].

The autoxidation of the four hydrocarbons under the same conditions were repeated in JSR-2, which was connected to GC at KAUST [32]. The temperature range is from 475 to 700 K. The design of the reactor and sampling for JSR-2 with volume of 76 cm³ are similar to those of Dagaut et al. [31]. JSR-2 was located in an oven and the temperature of the reactor was measured by a K-type thermocouple. Good temperature homogeneity was observed by moving the thermocouple along the centerline of the reactor. In this work, we used the JSR-2 experiment to correct the reaction temperature in JSR-1. The actual reaction temperature of JSR-1 was obtained by empirically correcting the recorded reactor temperature with a simple function i.e., $T_{\text{actual}}=1.04T_{\text{record}}$, which allows a temperature increase of ~ 20 K for the temperature range studied in this work.

The injection system (fuel vaporization, flow rate measurement of fuels and gases) in JSR-2 is similar to that of JSR-1. The products were sampled by a sonic-throat gas sampling probe located at the outlet of the reactor and connected to a mechanical vacuum pump. The pressure-drop across the orifice was sufficient to prevent further reactions in the sample transfer line. The sample gas was analyzed online using Agilent Refinery Gas Analysis (RGA) and Agilent 7890B GC. The Agilent RGA system, following ASTM D1945, D1946, and UOP 539 method, was used to quantify CO, CO₂, O₂, H₂, CH₄, ethylene, and propene during autoxidation of the four C₁₀ hydrocarbons. The Agilent 7890B system was equipped with a DB-1 column to measure *n*-decane, 2-methylnonane, 2,7-dimethyloctane, and *n*-butylcyclohexane. The uncertainty on reactant mole fraction is $\pm 5\%$, while that for the oxidation products is estimated to be $\pm 15\%$. Oxygenated intermediates were not

measured by GC in this work.

In addition, theoretical calculations were performed to estimate the photoionization cross sections of the key intermediates controlling the ignition process, such as C₁₀-alkene, C₁₀-cyclic ether, and C₁₀-keto-hydroperoxide, and C₁₀-keto-dihydroperoxides. Photoionization cross sections for systems where experimental information is not available are often estimated by analogy with similar species or via simple models, and the accuracy of such estimates is not typically known. In a recent study [27], the accuracy of a combined theoretical/experimental approach for predicting photoionization cross sections was tested. Briefly, in this approach the transition dipole moment is calculated using the frozen-core Hartree–Fock (FCHF) method and ePolyScat code developed by Lucchese and co-workers [33–36]. In the FCHF calculations, the geometries of the neutral species were optimized using M06-2X/cc-pVTZ, and their orbital energies were calculated using restricted HF/aug-cc-pVTZ. The computation of the Franck-Condon overlap envelope, which is difficult to determine accurately for systems with more than a few nonlocal modes, is avoided. Instead, “plateau” regions in the photoionization spectra around 1.0–1.5 eV above threshold are identified, where it is assumed that the photon energy is high enough to saturate the Franck–Condon transition envelope and low enough to avoid transitions to excited electronic states. The calculation shows that KHPs the Franck-Condon factor becomes unity (=1). That means, the intensity of the signal cannot increase further. When plateau regions are present, the computed transition dipole can be used as an estimate of the photoionization cross section.

3. Results and discussion

GC analyses were performed to quantify the mole fractions of reactants (the four C₁₀ hydrocarbons and O₂), CO, CO₂, ethylene, propene, methane, and hydrogen. These data from JSR-2 are valuable to examine the autoxidation reactivity of the four C₁₀ hydrocarbons. Furthermore, the detailed species pool measured in the SVUV-PI-MBMS experiments from JSR-1 were used to examine the autoxidation reaction mechanism of the four C₁₀ hydrocarbons. Kinetic models of *n*-decane, 2-methylnonane, and *n*-butylcyclohexane from LLNL and 2,7-dimethyloctane from

KAUST [7-9,29] were examined by comparison against the experimental data. Simulations were performed in CHEMKIN-PRO [37] using the perfectly stirred reactor module. The transient solver was used with an end time of 30 seconds to ensure converged solutions. The input conditions for simulations were identical to those in experiments.

3.1 Autoxidation reactivity of four C₁₀ hydrocarbons

The mole fraction profiles for *n*-decane, 2-methylnonane, 2,7-dimethyloctane, and *n*-butylcyclohexane measured from GC and SVUV-PI-MBMS are presented in Fig. 1. The results from the two JSRs with different analytic methods are in good agreement. The autoxidation starts from 525 K and the conversion of reactants increases until 625 K, where the negative temperature coefficient behavior (i.e., the reactivity decreases with increasing of temperature) appears.

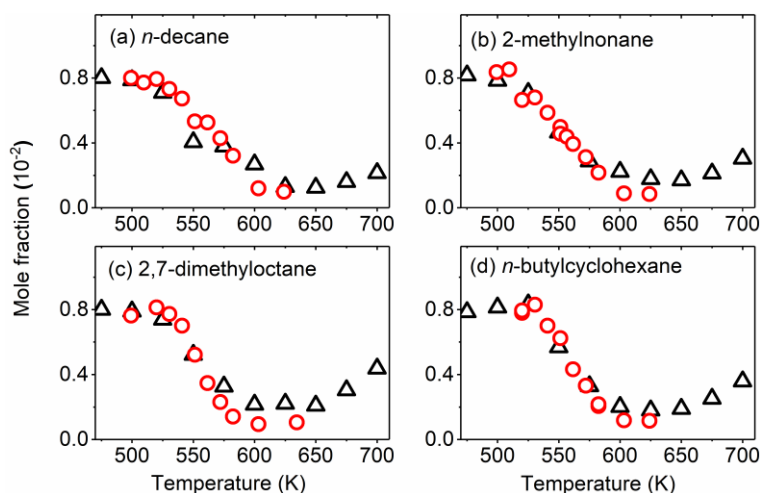


Figure 1. Mole fraction of *n*-decane, 2-methylnonane, 2,7-dimethyloctane, and *n*-butylcyclohexane measured in JSR-1 (open circle) and JSR-2 (open triangle).

The GC measured and model predicted mole fractions for the reactants (fuel and O₂), CO and CO₂, and two alkenes (C₂H₄ and C₃H₆) are presented in Fig. 2. The measurements reveal that the four hydrocarbons have similar reactivity under this work's experimental conditions. The trend of the reactivity for the four C₁₀ hydrocarbons is predicted by the models, however, the fuel reactivity in the low-temperature regime is over-predicted by the simulation, especially for *n*-decane, 2-methylnonane, and *n*-butylcyclohexane. Oxygen is also over-consumed while CO is over-predicted in the low-temperature regime. For CO₂, the mole fraction was under-predicted by a factor of 2-3 in all

cases. The analysis of the discrepancy between simulation and experiment is not the focus of this work, and can be done in a future work. The mole fraction of the species measured by GC is shown in **Table S1-S4**.

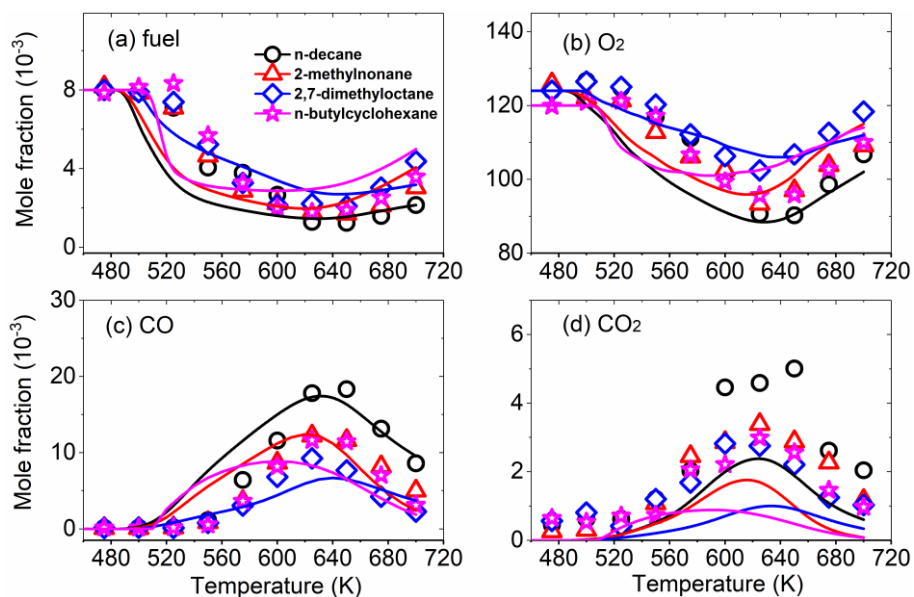


Figure 2. Mole fractions of four C₁₀ hydrocarbons, O₂, CO, and CO₂ measured in JSR-2 (open symbols). The lines represent simulations from LLNL and KAUST models [7-9,29].

It is well known that the autoxidation reactivity is controlled by the peroxy radical chemistry, which determines the concentrations of OH and HO₂ radicals. Sensitivity analysis of OH radical was investigated at 530 K, which corresponds to the largest deviation of the modeling versus experimental data. The analysis reveals that reactions influencing OH formation are directly related to the fuel low-temperature oxidation chemistry, such as the RO₂ radical isomerization, O₂ addition to QOOH radical, cyclization of QOOH, decomposition of KHP, and H-abstraction from the fuel by the OH radical (**Fig. S1 to S4**). We also analyzed the sensitive reactions for the fuel decay at the same temperature. The result reveals that the most sensitive reactions affecting the fuel conversion is the H-abstraction from the fuel by the OH radical (**Fig. S5 to S8**). In the experiments, OH and HO₂ radical was not measured due to their high reactivity and low concentration. Instead, key intermediates, such as alkenes, cyclic ethers, KHP, and more highly oxygenated species are investigated to understand fuel auto-ignition chemistry. Decomposition of these species lead to production of smaller radicals (OH, HO₂, etc.) that drive the system's reactivity [25].

3.2 Species pool of four C₁₀ hydrocarbons

Figure S9 displays the mass spectra in the range of 40-230 recorded during the autoxidation of *n*-decane, 2-methylnonane, 2,7-dimethyloctane, and *n*-butylcyclohexane autoxidation at ~560 K and at a photon energy of 10.5 eV. At this energy most of the intermediates formed during the autoxidation reaction could be ionized at this energy, except for some intermediates like formaldehyde and formic acid. The mass peaks correspond to hydrocarbons, oxygenates, and also the fragments. In this work, the photon energy at 9.5 eV, 10.5 eV, and 11.6 eV was selected to measure the intermediate distribution and avoid fragments. In general, the distribution of the autoxidation intermediates from the four hydrocarbons are very similar. A more detailed presentation of mass peaks of *n*-decane are presented in Fig. 3 and Fig. 4, except for those with nominal *m/z* of 66, 80, 94, 108, and 122, which are shown in **Fig. S10**. The detailed mass spectra for 2-methylnonane, 2,7-dimethyloctane, and *n*-butylcyclohexane are included in **Fig. S11-S19**, **Fig. S20-S28**, and **Fig. S29-S37**.

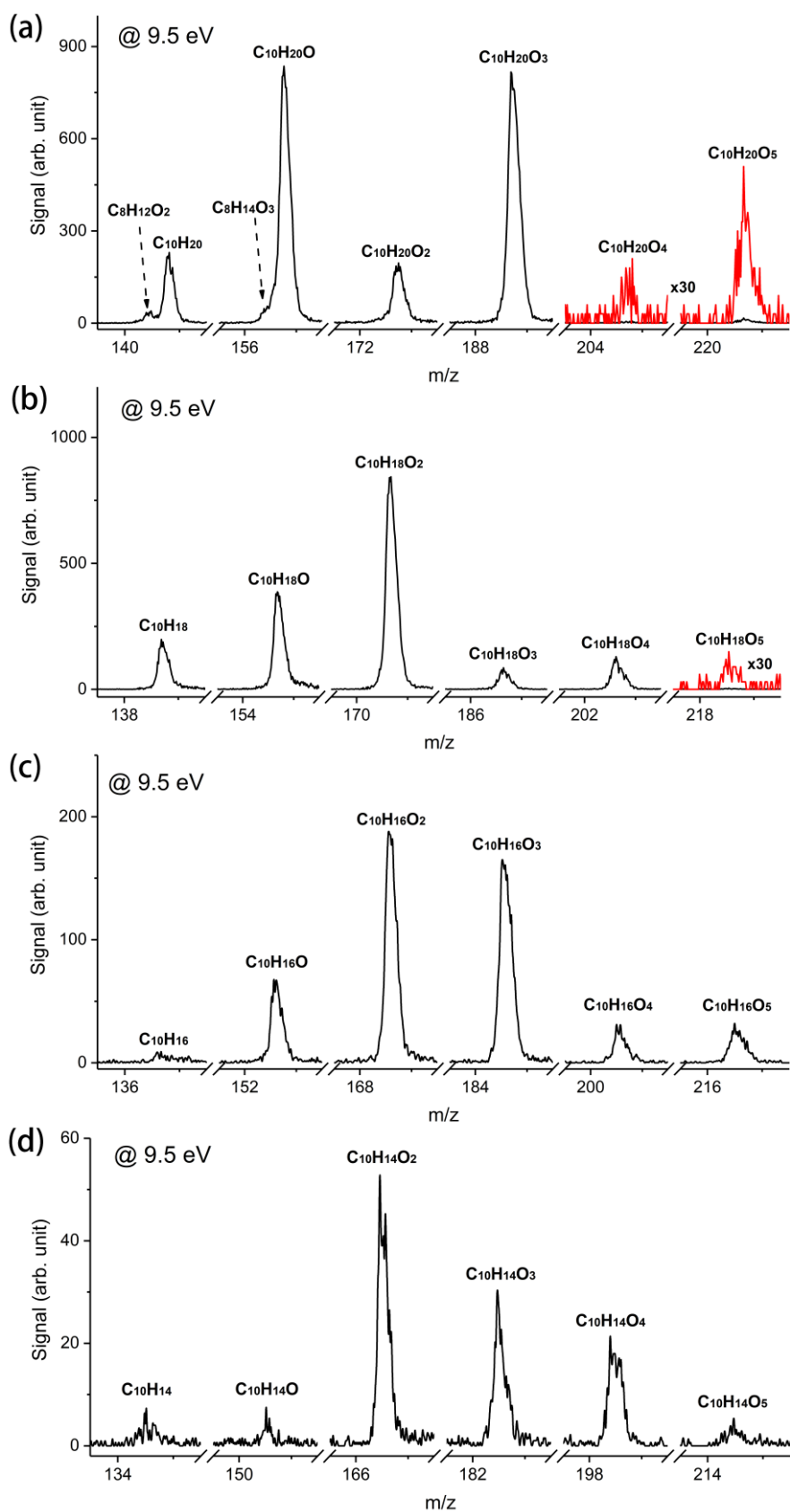


Figure 3. Molecules with ten carbon numbers measured during the autoxidation of *n*-decane at a reaction temperature of 551 K.

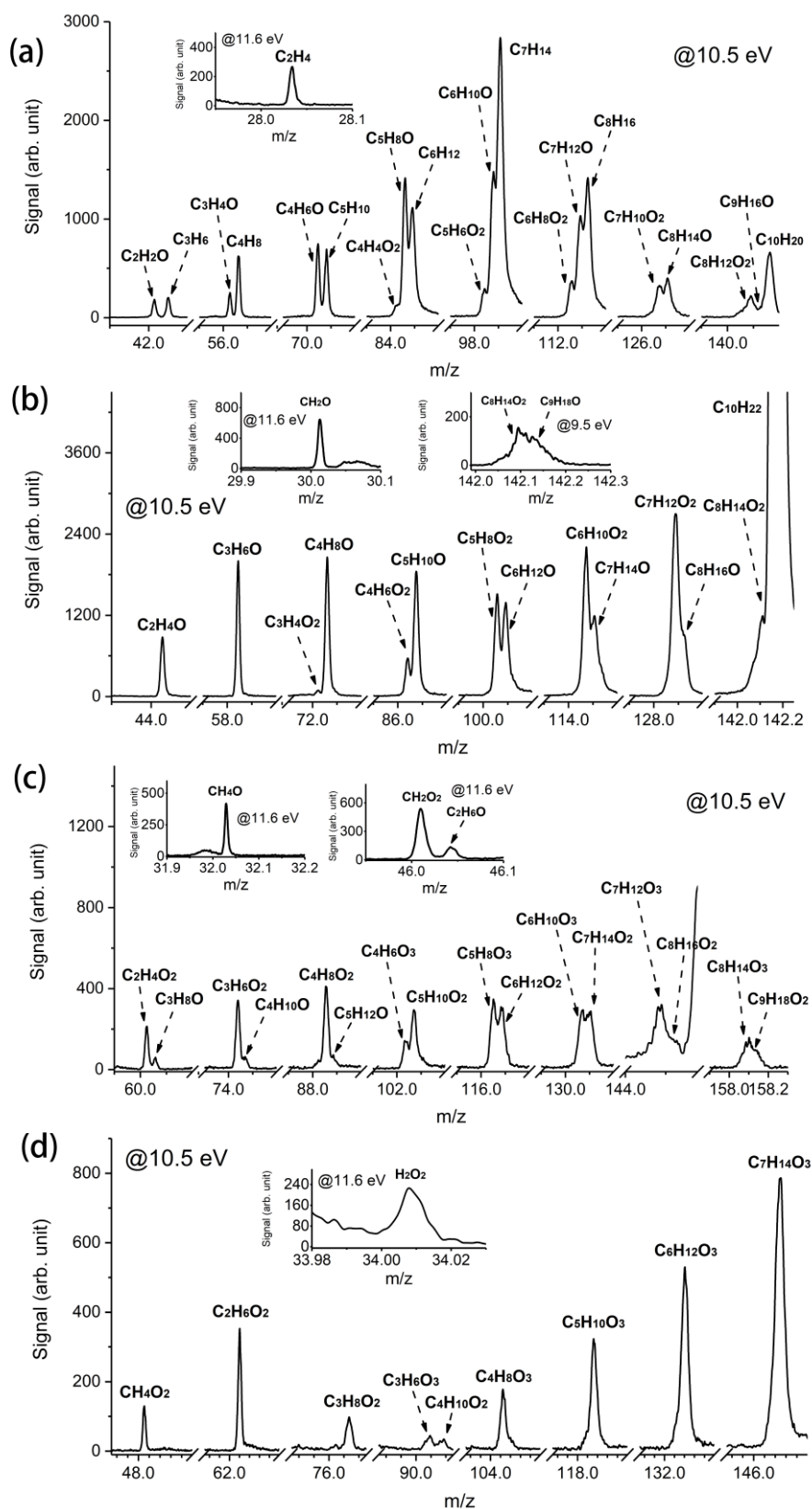


Figure 4. Molecules with less than ten carbon numbers measured during the autoxidation of *n*-decane at a reaction temperature of 551 K.

The distribution of the oxidation products during the oxidation of these four hydrocarbons is presented in **Table S5**. The mass resolution of the mass spectrometer is able to distinguish the C/H/O composition of oxidation intermediates, but it is not high enough to separate completely the hydrocarbon and oxygenate composition of the mass peak with a high nominal m/z (usually $> m/z$ 60). The results reveal that the autoxidation of the diesel surrogate components is much more complex than the literature study [11,18]. Lacking a comprehensive detection of the oxidation intermediates, the kinetic models developed from limited species information may not describe well the autoxidation chemistry of the transportation fuels. However, the challenging still exist such as separating completely the mass peaks, knowing their structures or the structures of the dominant isomers, and quantifying these complex intermediates.

Furthermore, we categorize the intermediate pool of *n*-decane, 2-methylnonane, 2,7-dimethyloctane, and *n*-butylcyclohexane autoxidation. The result are based on **Table S5**. Figure 5 presents the intermediates measured for *n*-decane autoxidation with molecular formulas of $C_xH_yO_z$ ($x \geq 1$). The major oxidation products like H_2 , CH_4 , CO , CO_2 , H_2O , as well as H_2O_2 are not shown. The species pool for 2-methylnonane, 2,7-dimethyloctane, and *n*-butylcyclohexane are shown in **Fig. S38**, **Fig. S39**, and **Fig. S40**. The autoxidation intermediate distribution for the four fuels is similar. They include 24 species with same number of carbon atoms as in the reactants, e.g., $C_{10}H_{y-2}O_z$ ($z=0-5$), $C_{10}H_{y-4}O_z$ ($z=0-5$), $C_{10}H_{y-6}O_z$ ($z=0-5$), and $C_{10}H_{y-8}O_z$ ($z=0-5$). Here, y equals 22 for *n*-decane, 2-methylnonane, and 2,7-dimethyloctane while y equals to 20 for *n*-butylcyclohexane. Other intermediates include C_nH_{2n-4} ($n=5-9$), C_nH_{2n-2} ($n=4-8$), C_nH_{2n} ($n=2-8$), $C_nH_{2n-6}O$ ($n=6-8$), $C_nH_{2n-4}O$ ($n=4-8$), $C_nH_{2n-2}O$ ($n=2-9$), $C_nH_{2n}O$ ($n=1-9$), $C_nH_{2n+2}O$ ($n=1-5$), $C_nH_{2n-4}O_2$ ($n=4-8$), $C_nH_{2n-2}O_2$ ($n=2-9$), $C_nH_{2n}O_2$ ($n=1-9$), $C_nH_{2n+2}O_2$ ($n=0-4$), $C_nH_{2n-2}O_3$ ($n=4-8$), $C_nH_{2n}O_3$ ($n=3-7$), and $C_nH_{2n-2}O_4$ ($n=6-8$). In addition, aromatic compounds C_nH_{2n-6} ($n=6-9$) were detected in the autoxidation of *n*-butylcyclohexane. Similar to *n*-heptane autoxidation [20], the intermediate species include mainly alkene, dienes, aldehyde/keto compounds, olefinic aldehyde/keto compounds, diones, cyclic ethers, peroxides, acids, and alcohols/ethers. Identification of the structure of some

intermediates could also refer to previous measurement for *n*-decane [11-13] and *n*-butylcyclohexane [18,19].

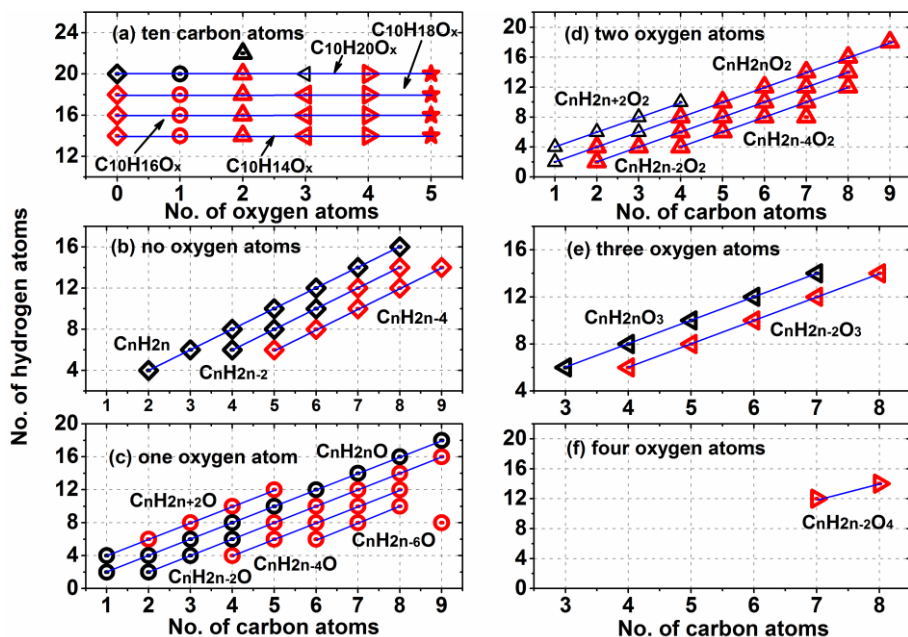
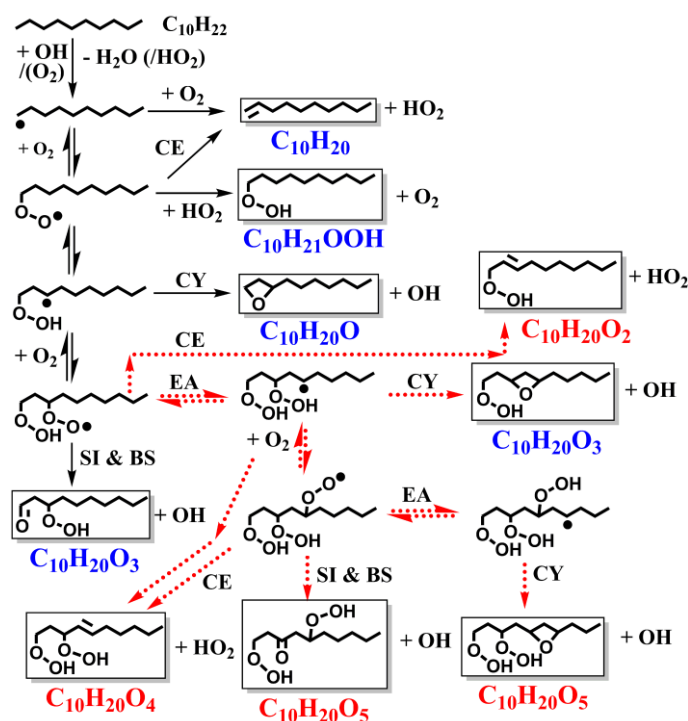


Figure 5. Intermediates detected by SVUV-PI-MBMS (labeled in black and red) during the autoxidation of *n*-decane. The species labeled in black are predicted by the LLNL model [7] with mole fraction higher than 1 ppm, while the species labeled in red are not included in the model/or the predicted concentration are lower than 1 ppm.

The black symbols in Fig. 5 and **Fig. S38, Fig. S39, and Fig. S40** are intermediates predicted by the kinetic models from LLNL and KAUST [7-9,29] with mole fraction higher than 1 ppm, which is the detection limit of the mass spectrometer in this work. We note that the isomers for a specific molecular formula are not distinguished, i.e., the symbols in Fig. 5 and **Fig. S38, Fig. S39, and Fig. S40** may contain more than one species. Specifically, four groups of C_{10} intermediates, $C_{10}H_{20}O_z$ ($z=0-5$), $C_{10}H_{18}O_z$ ($z=0-5$), $C_{10}H_{16}O_z$ ($z=0-5$), and $C_{10}H_{14}O_z$ ($z=0-5$) are observed in *n*-decane autoxidation experiments. However, the model only predicted four C_{10} intermediates, $C_{10}H_{20}$, $C_{10}H_{20}O$, $C_{10}H_{21}OOH$, and $C_{10}H_{20}O_3$ (Fig. 5a). They correspond to the species labeled in blue in Scheme 1, and the reaction pathways are given in the kinetic models. Here, the reaction channels for other C_{10} intermediates shown in Fig. 5a (i.e., those not currently predicted by the models) are discussed. The $C_{10}H_{20}O_2$, $C_{10}H_{20}O_4$, and $C_{10}H_{20}O_5$ could be formed by the reactions labeled by red dashed lines in Scheme 1, i.e., concerted elimination of $OOQOOH$ radical, the isomerization of

OOQOOH to P(OOH)₂ following a third O₂ addition reaction network. These reaction pathways have been recently confirmed in the autoxidation of hydrocarbon and oxygenated compounds [22-24]. Three other groups of intermediates, i.e., C₁₀H₁₈O_z (z=0-5), C₁₀H₁₆O_z (z=0-5) and C₁₀H₁₄O_z (z=0-5) could be formed from the bimolecular reactions of C₁₀H₂₀O_z (z=0-5) or the combination of radical intermediates. For example, as discussed in *n*-heptane cool flame chemistry [20], the bimolecular reactions of C₁₀H₂₀O_z (z=0-5) leads to intermediates C₁₀H₁₈O_z (z=0-5). Following the same logic, C₁₀H₁₆O_z (z=0-5) and C₁₀H₁₄O_z (z=0-5) could be formed.



Scheme 1. Reaction scheme for *n*-decane autoxidation initiated from the primary fuel radical. Representative structures of the intermediates are presented. The molecular formula labeled in red are measured from experiment while not predicted by the simulation. CE: concerted elimination, CY: cyclization, EA: extensive autoxidation, SI: standard isomerization, BS: beta-scission [22].

For the intermediates with less than ten carbon atoms, the important intermediates according to model predictions are C₂-C₈ alkenes (C_nH_{2n}), C₄-C₆ dienes (C_nH_{2n-2}), C₁-C₉ aldehyde/keto compounds (C_nH_{2n}O), C₂-C₄ unsaturated aldehyde/keto compounds (C_nH_{2n-2}O), C₁-C₄ alkyl hydroperoxides (C_nH_{2n+2}O₂), and C₃-C₇ keto-hydroperoxides (C_nH_{2n}O₃). In addition to these

common species, the measurements include intermediates with even higher degrees of unsaturation, such as those highlighted in red in Figs. 5b-5e. The reaction mechanism for these additional intermediates has seldom been investigated. Previous experiments with conventional analytical methods did not capture this complex species pool. In addition, identification of the structure of these species and their quantification is needed, which is challenging due to the lack of photoionization cross section data. Therefore, further analysis of the reaction mechanism and the structure of these intermediates is not carried out here. The readers can refer to the recent work on *n*-heptane oxidation [20], where the reaction mechanism and the probable structure of similar species were discussed in detail.

3.3 Quantification of key autoxidation intermediates

Measurements of the initial autoxidation intermediates from the SVUV-PI-MBMS experiment, especially KHP and keto-dihydroperoxide intermediates, are valuable to examine the kinetic models. However, their quantification is normally unfeasible due to the lack of photoionization cross sections (PICS). Recently, group additivity [13,38] and theoretical calculations [27,39] have been used to attempt estimating the PICS of the autoxidation intermediates. Moshhammer et al. [27] described a theoretical approach to calculate the PICS of intermediates that appeared in the autoxidation of dimethyl ether. Validation of the method with measured absolute PICS achieved an uncertainty of 2. The cases with poor Franck–Condon overlaps, excited electronic states of the photoionized cation, and fragmentation of the cation were discussed.

Here, the approach of Moshhammer et al. [27] was adopted to estimate the PICS of the autoxidation intermediates of *n*-heptane, e.g., alkene (C_7 -olefin), cyclic ether (C_7 -CE), alkenyl keto compound (C_7 -alkenyl keto), dione (C_7 -dione), keto-hydroperoxide (C_7 -KHP), diketo-hydroperoxide (C_7 -DKHP), and keto-dihydroperoxide (C_7 -KDHP). The C_7 oxygenates shown in Fig. 6 are the most represented structures for alkane autoxidation from model simulation [40] and kinetic analysis [20]. They were taken as model compounds to estimate the PICS for the C_{10} species with same functional groups, since the direct computation for C_{10} intermediates is computationally prohibitive given the

number of heavy atoms (ten carbon atoms and zero to five oxygen atoms). We assumed that the contribution to PICS includes two components, i.e., the contribution from the parent molecule and from the functional group (e.g., double bond, keto group, hydroperoxy group). Thus, the PICS for the oxidation intermediates with same functional group is directly related to the PICS of the parent molecule. The absolute PICS for *n*-heptane, *n*-decane, 2-methylnonane, 2,7-dimethyloctane, and *n*-butylcyclohexane is compared in **Fig. S41**. The results show that, except for 2,7-dimethyloctane, the PICS for other four hydrocarbons is close to each other at photoionization energy 1 eV and 1.5 eV above the ionization onset. Furthermore, the photoionization efficiency spectra for each class of oxidation intermediate in *n*-heptane, *n*-decane, 2-methylnonane, 2,7-dimethyloctane, and *n*-butylcyclohexane autoxidation is very close, especially from the ionization onset to 1 eV above the onset (**Fig. S41**). These observations indicate that using the PICS of model intermediates from *n*-heptane autoxidation to estimate the PICS of those produced from the four C₁₀ hydrocarbons autoxidation might be reasonable, although larger uncertainty may exist to estimate the PICS for the C₁₀ intermediates in 2,7-dimethyloctane autoxidation.

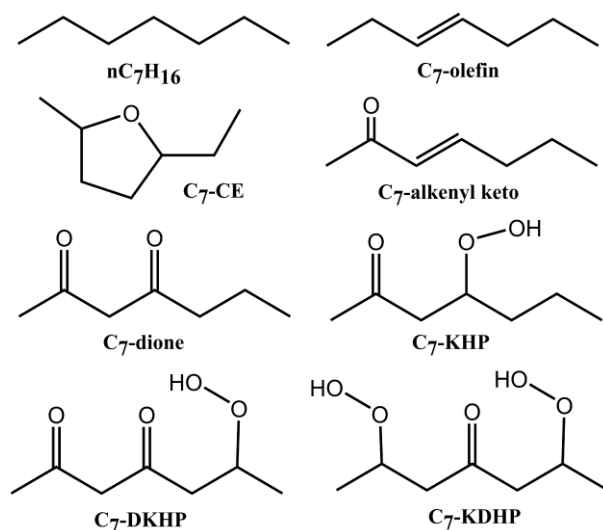


Figure 6. The structures of *n*-heptane and seven classes of intermediates from its autoxidation.

The calculated PICS for the eight molecules in Fig. 6 are presented in **Table S6**. The PICS at two photon energies, i.e., 1 eV and 1.5 eV above the ionization onset was calculated. First, we compared the PICS of *n*-heptane and C₇-olefin with literature measurements. Zhou et al. [41] measured the PICS for *n*-heptane with the value of 25 Mb and 28 Mb, at 1 eV and 1.5 eV above the

ionization onset, respectively. The calculated value is 8 Mb and 9 Mb, which are three times lower than the measurement. Yang et al. [42] measured the PICS for 1-hexene and trans-2-hexene. Reported PICS for 1-hexene at 1 eV and 1.5 eV above the ionization onset is ~10 Mb; for trans-2-hexene at 1 eV and 1.5 eV above the ionization onset is ~12 Mb. The calculated PICS for C₇-olefin is 37 Mb and 47 Mb at 1 eV and 1.5 eV above the ionization onset, which is three to four times higher than the measurement for the species with similar structure. These tests indicate that an uncertainty of a factor of ~4 may exist for the calculated PICS of these C₇ molecule, larger than a factor of ~2 for the C₁-C₃ species [27].

In the SVUV-PI-MBMS experiment, the temperature scan from 500-630 K was done at photon energies of 9.6, 10.5, and 11.6 eV. The mole fraction of the intermediates can be calculated from the reactant, since their initial mole fraction is known. The measured absolute PICS for 2-methylnonane, 2,7-dimethyloctane, and *n*-butylcyclohexane at 10.5 and 11.6 eV is shown in Table 1. We note that the PICS for these three C₁₀ hydrocarbons have not been reported in the literature. The photoionization efficiency curve for the seven classes of intermediates are shown in **Fig. S42**, where the ionization onset for each intermediate is indicated by the arrow. The PICS for these species at 1 eV and 1.5 eV above the ionization threshold was obtained from those in **Table S6**. Then, the PICS at 9.6 eV and/or 10.5 eV were obtained from the photoionization efficiency curve of each intermediate. The PICS for each kind of intermediate during the four C₁₀ hydrocarbon oxidation are close at 9.6 eV, as shown in **Table S7**. Their average values are given in Table 1.

Table 1. PICS of *n*-decane, 2-methylnonane (2MNN), 2,7-dimethyloctane (27DMOC), *n*-butylcyclohexane (NBCH), formic acid (FA) at 11.6 eV and 10.5 eV. The average value for olefin, cyclic ether (CE), alkenyl keto (AK), dione (DI), keto-hydroperoxide (KHP), diketo-hydroperoxide (DKHP), and keto-dihydroperoxide (KDHP) at 9.6 eV and/or 10.5 eV are also presented. Unit: Mb.

	<i>n</i> -decane	2MNN	27DMOC	NBCH	FA	olefin	CE	AK	DI	KHP	DKHP	KDHP
11.6 eV	38	30	14	38	9.7							
10.5 eV	22	18	7	24	--					6.26		
9.6 eV						37.0	14.2	5.1	2.9	3.0	1.5	0.7

First, the mole fraction of KHP was calculated at 10.5 eV using each reactant (i.e., C₁₀

hydrocarbon) as internal standard. Then, the mole fractions of other intermediates were calculated at 9.6 eV using KHP as the internal standard. The near threshold ionization at 9.6 eV mitigates the effects of fragmentation, but the fragments from KHP, DKHP, and KDHP were observed. Thus, for the quantification of these peroxides, the used signals are the total signals by including its fragments, for example those fragmented via the loss of $-OH$ or $-OOH$. The total uncertainty for the calculated mole fraction for the seven classes of C_{10} intermediates is tentatively assigned as a factor of 10, due to the many isomers that exist for the seven classes of C_{10} intermediates, the uncertainty of the PICS for each reactant, the uncertainty of estimating PICS of C_{10} intermediates from C_7 intermediates, and the uncertainty of PICS calculation for the C_7 intermediates. In addition, the mole fraction of formic acid was calculated at 11.6 eV using the reactant as internal standard; the uncertainty for formic acid mole fraction is estimated to be $\pm 50\%$ since its PICS was measured in the literature [43].

The mole fractions of C_{10} -olefin, C_{10} -CE, C_{10} -KHP, and C_{10} -KDHP are presented in Fig. 7. Although large uncertainty may exist for quantification, the mole fractions of C_{10} -olefin, C_{10} -CE, C_{10} -KHP are on the order of the models predictions. Their formation mechanism can be explained by the similar reaction pathways in Scheme 1. On the other hand, the isomerization of $OOQOOH$ followed by third O_2 addition in Scheme 1 was not included in the kinetic models and the models could not predict C_{10} -KDHP in Fig. 7d.

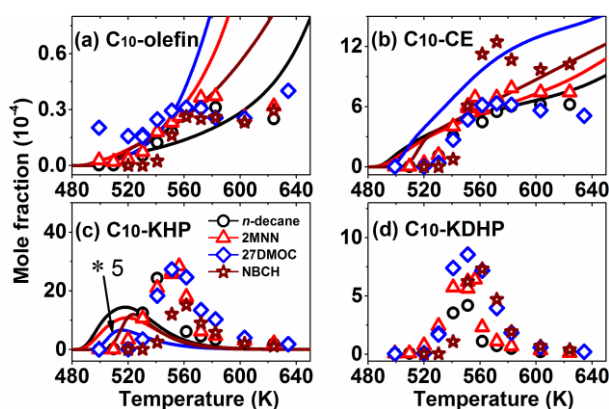
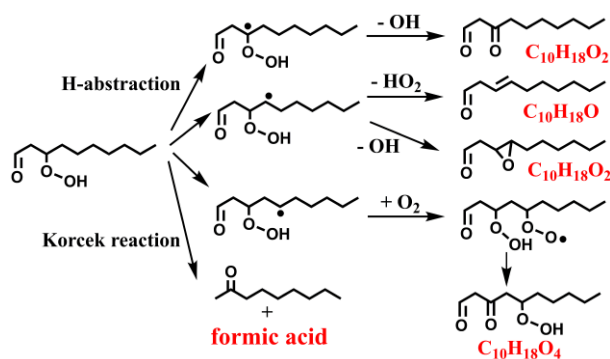


Figure 7. Mole fractions of C_{10} -olefin, C_{10} -CE, C_{10} -KHP, and C_{10} -KDHP. Symbols are experimental measurements and lines are predictions by LLNL and KAUST models [7-9,29]. The simulation in Fig. 7c for 2,7-dimethyloctane was increased by a factor of 5.

The over-prediction of the reactivity by the models is also reflected by the earlier production of

KHP in Fig. 7c. The dominant consumption pathway for this intermediate is the $-O-OH$ bond dissociation to release OH radical, playing pivotal role of chain-branching step in auto-ignition. Other pathways for KHP, such as its bimolecular reaction and Korcek reaction produce less OH radical. Some theoretical studies have investigated these additional reaction pathways [44-46]. Scheme 2 presents examples of these pathways, which lead to alkenyl keto ($C_{10}H_{18}O$), dione ($C_{10}H_{18}O_2$), keto cyclic ether ($C_{10}H_{18}O_2$), diketo-hydroperoxide ($C_{10}H_{18}O_4$), and formic acid.



Scheme 2. Formation of alkenyl keto, dione/keto cyclic ether, diketo-hydroperoxide from the bimolecular reactions of KHP and formation of formic acid from the Korcek reaction of KHP.

The mole fractions of the aforementioned four classes of intermediates (Fig. 8), are of the order of 100 to 1000 ppm. The kinetic models do not include the bimolecular reactions of KHP and thus cannot predict the formation of C₁₀-DKHP, C₁₀-dione/keto cyclic ether, and C₁₀-alkenyl keto. The simulated mole fraction of formic acid in Fig. 8d is a factor of 10 higher than the measurement. Instead of the Korcek reaction, the kinetic models suggest that formic acid comes from the OH radical addition to formaldehyde and a subsequent β -C-H scission, which was also reported in previous work on butanol oxidation in JSR [47]. However, from recent work on *n*-heptane [20], the OH radical addition to formaldehyde was shown to be unfavorable compared to the H-abstraction of formaldehyde by OH radical. The unrealistic rate constant for this reaction in the LLNL and KAUST models could be the main reason for the over-prediction.

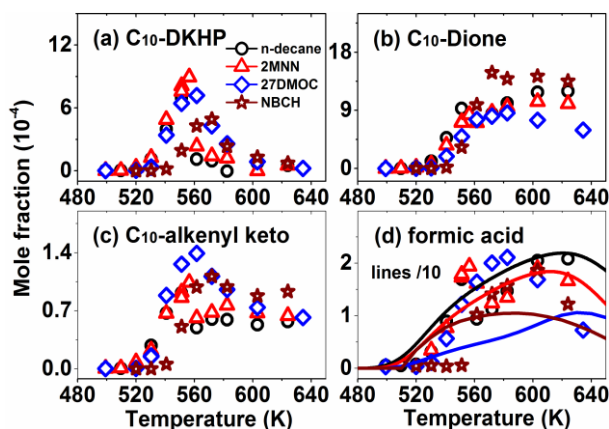


Figure 8. Mole fractions of C₁₀-DKHP, C₁₀-dione, C₁₀-alkenyl keto, and formic acid. Symbols are experimental measurements and lines are predictions by LLNL and KAUST models [7-9,29].

4. Summary and conclusions

The cool flame chemistry of four diesel surrogate compounds, *n*-decane, 2-methylnonane, 2,7-dimethyloctane, and *n*-butylcyclohexane, was investigated in two JSR at atmospheric pressure. The mole fraction profiles for the reactants, CO, CO₂, H₂, CH₄, C₂H₄, and C₃H₆ were measured by the GC analysis, and the detailed species pool for their autoxidation was examined by SVUV-PI-MBMS. The results show that the four C₁₀ hydrocarbons have similar autoxidation reactivity and similar distribution of the autoxidation intermediates. The intermediates can be categorized in two groups, i.e., intermediates with the same carbon number of the reactant, and intermediates with less carbon number of the reactant. Specifically, the intermediates with the same carbon number of the reactant include 24 species, i.e., C₁₀H_{y-2}O_z (z=0-5), C₁₀H_{y-4}O_z (z=0-5), C₁₀H_{y-6}O_z (z=0-5), and C₁₀H_{y-8}O_z (z=0-5). Here, y equals 22 for *n*-decane, 2-methylnonane, and 2,7-dimethyloctane while y equals to 20 for *n*-butylcyclohexane. Intermediates with less carbon number of the reactant are C_nH_{2n-4} (n=5-9), C_nH_{2n-2} (n=4-8), C_nH_{2n} (n=2-8), C_nH_{2n-6}O (n=6-8), C_nH_{2n-4}O (n=4-8), C_nH_{2n-2}O (n=2-9), C_nH_{2n}O (n=1-9), C_nH_{2n+2}O (n=1-5), C_nH_{2n-4}O₂ (n=4-8), C_nH_{2n-2}O₂ (n=2-9), C_nH_{2n}O₂ (n=1-9), C_nH_{2n+2}O₂ (n=0-4), C_nH_{2n-2}O₃ (n=4-8), C_nH_{2n}O₃ (n=3-7), and C_nH_{2n-2}O₄ (n=6-8). In the case of *n*-butylcyclohexane autoxidation, aromatic compounds C_nH_{2n-6} (n=6-9) were also detected.

The experimental data were used to examine the kinetic models available in the literature for

the four fuels, which over-predicted their autoxidation reactivity. Moreover, the species pool predicted by the models is significantly less than experimental observations, due to the lack of reaction pathways and/or too low concentration as predicted by simulation. The model was also examined by several key autoxidation intermediates, highlighting the initial oxidation of the reactants and the bimolecular reactions of KHP. Apart from the third O₂ addition network, we proposed that the bimolecular reactions of KHP + OH, leading to alkenyl keto, dione, and keto cyclic ether, need to be considered in the kinetic models.

To quantify the key autoxidation intermediates, their PICS was estimated from a theoretical approach, which was used in the literature to estimate the PICS of C₁-C₂ molecules. However, uncertainties of a factor of 4 were found when applying this approach to calculate the PICS of the molecules with seven carbon number. The source of this increased error for larger systems is unclear, and improved theoretical methods are needed to reduce error in the computed transition dipole as well as to compute Franck-Condon overlap envelopes for systems with multiple torsions.

Acknowledgements

We would like to thank Dr. Kuiwen Zhang and Dr. William J. Pitz for sharing the *n*-butylcyclohexane kinetic model. This work was supported by: National Natural Science Foundation of China (51976208); King Abdullah University of Science and Technology (KAUST), Office of Sponsored Research (OSR) under Award No. OSR-2016-CRG5-3022; KAUST Clean Fuels Consortium (KCFC) and its member companies; Director, Office of Energy Research, Office of Basic Energy Sciences (BES), Chemical Sciences Division of the U.S. Department of Energy (USDOE), Gas Phase Chemical Physics Program, under Contract No. DE-AC02-05CH11231; and European Research Council under FP7/2007-2013/ERC Grant 291049-2G-CSafe (P.D.). The Advanced Light Source is supported by the Director, Office of Basic Energy Sciences, of the U.S. Department of Energy under Contract No. DE-AC02-05CH11231. Sandia National Laboratories is a

multimission laboratory managed and operated by National Technology and Engineering Solutions of Sandia, LLC., a wholly owned subsidiary of Honeywell International, Inc., for the U.S. Department of Energy's National Nuclear Security Administration under contract DE-NA0003525. The work at Argonne was supported by the U. S. Department of Energy, Office of Basic Energy Sciences, Division of Chemical Sciences, Geosciences, and Biosciences, under Contract Number DE-AC02-06CH11357.

References

- [1] W.J. Pitz, C.J. Mueller, Recent progress in the development of diesel surrogate fuels, *Prog. Energy Combust. Sci.* 37 (2011) 330-350.
- [2] S. Saxena, I.D. Bedoya, Fundamental phenomena affecting low temperature combustion and HCCI engines, high load limits and strategies for extending these limits, *Prog. Energy Combust. Sci.* 39 (2013) 457-488.
- [3] Z. Wang, O. Herbinet, N. Hansen, F. Battin-Leclerc, Exploring hydroperoxides in combustion: History, recent advances and perspectives, *Prog. Energy Combust. Sci.* 73 (2019) 132-181.
- [4] W. Yuan, Y. Li, F. Qi, Challenges and perspectives of combustion chemistry research, *Sci. China Chem.* 60 (2017) 1391-1401.
- [5] Y. Ju, C.B. Reuter, O.R. Yehia, T.I. Farouk, S.H. Won, Dynamics of cool flames, *Prog. Energy Combust. Sci.* 75 (2019) 100787.
- [6] M. Sarathy, A. Farooq, G.T. Kalghatgi, Recent progress in gasoline surrogate fuels, *Prog. Energy Combust. Sci.* 65 (2018) 67-108.
- [7] C.K. Westbrook, W.J. Pitz, O. Herbinet, H.J. Curran, E.J. Silke, A comprehensive detailed chemical kinetic reaction mechanism for combustion of n-alkane hydrocarbons from n-octane to n-hexadecane, *Combust. Flame* 156 (2009) 181-199.
- [8] S.M. Sarathy, C.K. Westbrook, M. Mehl, W.J. Pitz, C. Togbé, P. Dagaut, H. Wang, M.A. Oehlschlaeger, U. Niemann, K. Seshadri, P.S. Veloo, C. Ji, F.N. Egolfopoulos, T. Lu, Comprehensive chemical kinetic modeling of the oxidation of 2-methylalkanes from C7 to C20, *Combust. Flame* 158 (2011) 2338-2357.
- [9] S. Li, S.M. Sarathy, D.F. Davidson, R.K. Hanson, C.K. Westbrook, Shock tube and modeling study of 2,7-dimethyloctane pyrolysis and oxidation, *Combust. Flame* 162 (2015) 2296-2306.
- [10] N. Liu, S.M. Sarathy, C.K. Westbrook, F.N. Egolfopoulos, Ignition of non-premixed counterflow flames of octane and decane isomers, *Proc. Combust. Inst.* 34 (2013) 903-910.
- [11] P. Dagaut, M. Reuillon, M. Cathonnet, D. Voisin, High pressure oxidation of normal decane and kerosene in dilute conditions from low to high temperature, *J. Chim. Phys.* 92 (1995) 47-76.
- [12] O. Herbinet, B. Husson, M. Ferrari, P.-A. Glaude, F. Battin-Leclerc, Low temperature oxidation of benzene and toluene in mixture with n-decane, *Proc. Combust. Inst.* 34 (2013) 297-305.
- [13] A. Rodriguez, O. Herbinet, X. Meng, C. Fittschen, Z. Wang, L. Xing, L. Zhang, F. Battin-Leclerc, Hydroperoxide measurements during the low-temperature gas phase oxidation of n-heptane and n-decane, *J. Phys. Chem. A* 121 (2017) 1861-1876.
- [14] Z. Wang, S.Y. Mohamed, L. Zhang, K. Moshhammer, D.M. Popolan-Vaida, V.S. Bhavani Shankar, A. Lucassen, L. Ruwe, N. Hansen, P. Dagaut, S.M. Sarathy, New insights into the low-temperature oxidation of 2-methylhexane, *Proc. Combust. Inst.* 36 (2017) 373-382.

- [15] F. Karsenty, S.M. Sarathy, C. Togbé, C.K. Westbrook, G. Dayma, P. Dagaut, M. Mehl, W.J. Pitz, Experimental and Kinetic Modeling Study of 3-Methylheptane in a Jet-Stirred Reactor, *Energy Fuels* 26 (2012) 4680-4689.
- [16] S.M. Sarathy, T. Javed, F. Karsenty, A. Heufer, W. Wang, S. Park, A. Elwardany, A. Farooq, C.K. Westbrook, W.J. Pitz, M.A. Oehlschlaeger, G. Dayma, H.J. Curran, P. Dagaut, A comprehensive combustion chemistry study of 2,5-dimethylhexane, *Combust. Flame* 161 (2014) 1444-1459.
- [17] B. Husson, O. Herbinet, P.A. Glaude, S.S. Ahmed, F. Battin-Leclerc, Detailed Product Analysis during Low- and Intermediate-Temperature Oxidation of Ethylcyclohexane, *J. Phys. Chem. A* 116 (2012) 5100-5111.
- [18] R.H. Natelson, M.S. Kurman, N.P. Cernansky, D.L. Miller, Low temperature oxidation of n-butylcyclohexane, *Combust. Flame* 158 (2011) 2325-2337.
- [19] O. Herbinet, B. Husson, H. Le Gall, F. Battin-Leclerc, Comparison study of the gas-phase oxidation of alkylbenzenes and alkylcyclohexanes, *Chem. Eng. Sci.* 131 (2015) 49-62.
- [20] Z. Wang, B. Chen, K. Moshhammer, D.M. Popolan-Vaida, S. Sioud, V.S.B. Shankar, D. Vuilleumier, T. Tao, L. Ruwe, E. Brüauer, N. Hansen, P. Dagaut, K. Kohse-Höinghaus, M.A. Raji, S.M. Sarathy, n-Heptane cool flame chemistry: Unraveling intermediate species measured in a stirred reactor and motored engine, *Combust. Flame* 187 (2018) 199-216.
- [21] Z. Wang, L. Zhang, K. Moshhammer, D.M. Popolan-Vaida, V.S. Bhavani Shankar, A. Lucassen, C. Hemken, C.A. Taatjes, S.R. Leone, K. Kohse-Höinghaus, N. Hansen, P. Dagaut, S.M. Sarathy, Additional chain-branching pathways in the low-temperature oxidation of branched alkanes, *Combust. Flame* 164 (2016) 386-396.
- [22] Z. Wang, D.M. Popolan-Vaida, B. Chen, K. Moshhammer, S. Mohamed, H. Wang, S. Sioud, M.A. Raji, K. Kohse-Höinghaus, N. Hansen, P. Dagaut, S.R. Leone, Sarathy, S. Mani, Unraveling the structure and chemical mechanisms of highly oxygenated intermediates in oxidation of organic compounds, *Proc. Natl. Acad. Sci. USA* 114 (2017) 13102-13107.
- [23] L.-S. Tran, J. Wullenkord, Y. Li, O. Herbinet, M. Zeng, F. Qi, K. Kohse-Höinghaus, F. Battin-Leclerc, Probing the low-temperature chemistry of di-n-butyl ether: Detection of previously unobserved intermediates, *Combust. Flame* 210 (2019) 9-24.
- [24] J. Zou, X. Zhang, Y. Li, L. Ye, L. Xing, W. Li, C. Cao, Y. Zhai, F. Qi, J. Yang, Experimental and kinetic modeling investigation on ethylcyclohexane low-temperature oxidation in a jet-stirred reactor, *Combust. Flame* 214 (2020) 211-223.
- [25] E.-A. Tingas, Z. Wang, S. Mani Sarathy, H.G. Im, D.A. Goussis, Chemical kinetic insights into the ignition dynamics of n-hexane, *Combust. Flame* 188 (2018) 28-40.
- [26] Z. Wang, M.S. Sarathy, Third O₂ addition reactions promote the low temperature ignition of n-alkanes, *Combust. Flame* 165 (2016) 364-372.
- [27] K. Moshhammer, A.W. Jasper, D.M. Popolan-Vaida, Z. Wang, V.S. Bhavani Shankar, L. Ruwe, C.A. Taatjes, P. Dagaut, N. Hansen, Quantification of the Keto-Hydroperoxide (HOOCH₂OCHO) and Other Elusive Intermediates during Low-Temperature Oxidation of Dimethyl Ether, *J. Phys. Chem. A* 120 (2016) 7890-7901.
- [28] F. Qi, Combustion chemistry probed by synchrotron VUV photoionization mass spectrometry, *Proc. Combust. Inst.* 34 (2013) 33-63.
- [29] K. Zhang, C. Conroy, J. Bugler, W. Pitz, H.J. Curran, M. Mehl, S. Wagnon, G. Kukkadapu, An experimental and kinetic modeling study of n-butylcyclohexane and its mixture with n-heptan, 10th International Conference on Chemical Kinetics COM031 (2017).
- [30] K. Moshhammer, A.W. Jasper, D.M. Popolan-Vaida, A. Lucassen, P. Diévar, H. Selim, A.J. Eskola, C.A. Taatjes, S.R. Leone, S.M. Sarathy, Y. Ju, P. Dagaut, K. Kohse-Höinghaus, N. Hansen, Detection and Identification of the Keto-Hydroperoxide (HOOCH₂OCHO) and Other Intermediates during Low-Temperature Oxidation of Dimethyl Ether, *J. Phys. Chem. A* 119 (2015) 7361-7374.
- [31] P. Dagaut, M. Cathonnet, J.P. Rouan, R. Foulatier, A. Quilgars, J.C. Boettner, F. Gaillard, H. James, A jet-stirred reactor for kinetic studies of homogeneous gas-phase reactions at pressures up to ten atmospheres (1 MPa), J.

- Phys. E: Sci. Instrum. 19 (1986) 207–209.
- [32] B. Chen, Z. Wang, J.-Y. Wang, C. Togbé, P.E. Álvarez Alonso, M. Almalki, M. Mehl, W.J. Pitz, S.W. Wagnon, K. Zhang, G. Kukkadapu, P. Dagaut, S.M. Sarathy, Exploring gasoline oxidation chemistry in jet stirred reactors, *Fuel* 236 (2017) 1282-1292.
- [33] R.R. Lucchese, N. Sanna, A.P.P. Natalense, F.A. Gianturco, ePolyScat, version E3.
- [34] F.A. Gianturco, R.R. Lucchese, N. Sanna, Calculation of low - energy elastic cross sections for electron - CF₄ scattering, *J. Chem. Phys.* 100 (1994) 6464-6471.
- [35] A.P.P. Natalense, R.R. Lucchese, Cross section and asymmetry parameter calculation for sulfur 1s photoionization of SF₆, *J. Chem. Phys.* 111 (1999) 5344-5348.
- [36] B. Gans, S. Boye-Peronne, M. Broquier, M. Delsaut, S. Douin, C.E. Fellows, P. Halvick, J.-C. Loison, R.R. Lucchese, D. Gauyacq, Photolysis of methane revisited at 121.6 nm and at 118.2 nm: quantum yields of the primary products, measured by mass spectrometry, *Phys. Chem. Chem. Phys.* 13 (2011) 8140-8152.
- [37] CHEMKIN-PRO 15112, Reaction Design: San Diego, (2012).
- [38] A. Rodriguez, O. Herbinet, Z. Wang, F. Qi, C. Fittschen, P.R. Westmoreland, F. Battin-Leclerc, Measuring hydroperoxide chain-branching agents during *n*-pentane low-temperature oxidation, *Proc. Combust. Inst.* 36 (2017) 333–342.
- [39] C. Huang, B. Yang, F. Zhang, Calculation of the absolute photoionization cross-sections for C1–C4 Criegee intermediates and vinyl hydroperoxides, *J. Chem. Phys.* 150 (2019) 164305.
- [40] K. Zhang, C. Banyon, J. Bugler, H.J. Curran, A. Rodriguez, O. Herbinet, F. Battin-Leclerc, C. B'Chir, K.A. Heufer, An updated experimental and kinetic modeling study of *n*-heptane oxidation, *Combust. Flame* 172 (2016) 116-135.
- [41] Z.Y. Zhou, L.D. Zhang, M.F. Xie, Z.D. Wang, D.N. Chen, F. Qi, Determination of absolute photoionization cross-sections of alkanes and cyclo-alkanes, *Rapid Commun. Mass Spectrom.* 24 (2010) 1335-1342.
- [42] B. Yang, J. Wang, T.A. Cool, N. Hansen, S. Skeen, D.L. Osborn, Absolute photoionization cross-sections of some combustion intermediates, *Int. J. Mass Spectrom.* 309 (2012) 118-128.
- [43] T.A. Cool, J. Wang, K. Nakajima, C.A. Taatjes, A. McIlroy, Photoionization cross sections for reaction intermediates in hydrocarbon combustion, *Int. J. Mass Spectrom.* 247 (2005) 18-27.
- [44] A. Jalan, I.M. Alecu, R. Meana-Pañeda, J. Aguilera-Iparraguirre, K.R. Yang, S.S. Merchant, D.G. Truhlar, W.H. Green, New Pathways for Formation of Acids and Carbonyl Products in Low-Temperature Oxidation: The Korcek Decomposition of γ -Ketohydroperoxides, *J. Am. Chem. Soc.* 135 (2013) 11100-11114.
- [45] E. Ranzi, C. Cavallotti, A. Cuoci, A. Frassoldati, M. Pelucchi, T. Faravelli, New reaction classes in the kinetic modeling of low temperature oxidation of *n*-alkanes, *Combust. Flame* 162 (2015) 1679–1691.
- [46] L. Xing, J.L. Bao, Z. Wang, F. Zhang, D.G. Truhlar, Degradation of Carbonyl Hydroperoxides in the Atmosphere and in Combustion, *J. Am. Chem. Soc.* 139 (2017) 15821-15835.
- [47] S.M. Sarathy, S. Vranckx, K. Yasunaga, M. Mehl, P. Oßwald, W.K. Metcalfe, C.K. Westbrook, W.J. Pitz, K. Kohse-Höinghaus, R.X. Fernandes, H.J. Curran, A comprehensive chemical kinetic combustion model for the four butanol isomers, *Combust. Flame* 159 (2012) 2028-2055.